Asymptotic Modeling of Nonlinear Bending and Buckling Behavior of Carbon Nanotubes.

Sathiskumar A. Ponnusami*
University of Oxford, Oxford, OX1 3PJ, United Kingdom
Mohit Gupta †
Georgia Institute of Technology, Atlanta, Georgia 30332-0150
Dineshkumar Harursampath‡
Indian Institute of Science, Bangalore, 560012, India

The present work investigates the nonlinear bending and buckling behavior of Carbon Nano-Tubes (CNTs) using Variational Asymptotic Method (VAM). Considering a CNT as a slender beam structure, an asymptotically-correct nonlinear continuum beam model is presented. Through the resulting nonlinear moment-curvature relationship, the model captures the phenomenon of ovalization of the cross-sections and local buckling of the CNT, which arises due to their geometrical nature. Further studies are performed in order to explore the effect of CNT wall thickness on the nonlinear bending behavior of the CNT structure. It is shown that the continuum modeling approach can capture the ovalization and further localization of the CNT deformation under bending. The study aims to provide a reduced-order modeling framework analyzing the inherent nonlinearities associated with the geometrical nature of CNTs.

Nomenclature

$\mathbf{A}_i$	=	Polar basis for deformed geometry
a_i	=	Polar basis for undeformed geometry
$\mathbf{B}_i$	=	Cartesian basis for deformed geometry
$\mathbf{b}_i$	=	Cartesian basis for undeformed geometry
C_{ij}^{Bb}	=	rotation matrix from frame b to B
$\mathcal{D}$	=	material matrix 3-D stiffness
e_1	=	column matrix, $\lfloor 1\ 0\ 0 \rfloor^T$
$\mathbf{G}_k$	=	covariant base vectors of deformed configuration
$\mathbf{g}^k$	=	contravariant base vectors of undeformed configuration

*Postdoctoral Researcher, Solid Mechanics and Materials Engineering, Department of Engineering Science.
†Postdoctoral Fellow, Daniel Guggenheim School of Aerospace Engineering, Member, AIAA.
‡Associate Professor, Founder and Head-NMCAD Laboratory, Department of Aerospace Engineering.

h = wall thickness

K = column matrix of deformed tube twist and curvature measures

l = characteristic wavelength of deformation

R = characteristic dimension of cross section defining mean radius of cross section

$\mathbf{R}$ = position vector of points along deformed tube reference curve

$\mathbf{r}$ = position vector of points along undeformed tube reference curve

U = strain energy density

u = column matrix of displacement variables along b_i

u_i = 3-D displacement variables along b_i

w_i = 2-D warping variables for a cross section along b_i, averaged over the tube thickness

$\overline{w_i}$ = 3-D warping variables along b_i

x_1 = Cartesian coordinate along the reference line of an undeformed tube

x_2, x_3 = cross-sectional Cartesian coordinates

y_2, y_3 = cross-sectional polar coordinates

Γ_{ij} = 3-D strains

$\gamma_1 1$ = 1-D beam generalized extensional strain measures

Δ_α = Unknown variation in in-surface warping variables; $\alpha = 1, 2$

$\epsilon_{\alpha\beta}$ = membrane force strain measures

κ_i = 1-D beam twist and curvature measures

$\rho_{\alpha\beta}$ = membrane moment strain measures

A = mixed-basis components of deformation gradient tensor

$O(\,)$ = order of magnitude of a quantity

$\hat{(\,)}$ = position vector of arbitrary points in a beam

$\tilde{(\,)}$ = corresponding skew-symmetric matrix

$(\,)'$ = derivative with respect to x_1

$(\,)^T$ = Transpose of a matrix (square or column)

$\overline{(\,)}$ = a single variable as quantity

I. Introduction

Recent research focuses on development and characterization of CNTs on one hand while, on the other hand, CNTs are increasingly used as one of the reinforcing phases in matrix materials in order to enhance the mechanical performance of the structure and its tailorability. CNTs are thin-walled slender structures possessing very high stiffness and strength

along their length. At the same time, they have highly flexible cross-sections. Because of such flexibility as well as their thin, slender and hollow cylindrical structure, as shown in Fig. 1, they undergo large elastic bending deformation (under typical external loads acting on their parent structure) leading to the ovalization of their cross-sections. This phenomenon changes the effective bending stiffness of the CNT and hence the moment-curvature relationship. In addition, under such bending stresses, the thin-walled cylindrical tube may be subjected to local buckling which in turn affects the global mechanical behavior of the structure.

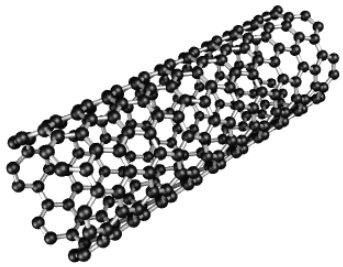

Fig. 1 Schematic of a carbon nanotube

When a matrix material, say epoxy, is reinforced with CNT, the above-discussed structural characteristics of the latter will influence the overall mechanical behavior of the composites. For example, the ovalization and buckling of the CNT could induce debonding of CNT with the surrounding matrix phase ultimately leading to degradation of overall structural stiffness and strength. Thus, it is an important to address such nonlinearities and instabilities associated with the geometrical nature of the CNT. More importantly, stand-alone CNTs were explored for its potential usage as sensors [1]. At times, long CNTs are grown over the surface of fibers for developing hybrid composite architectures [2]. In such cases, individual strands of carbon nanotubes are subjected to Mode I fractures (fracture caused of forces perpendicular to the length of a slender structure applied in opposite directions on the top and bottom faces, also known as the opening mode) and buckling when they interact with strands grown on other surfaces. Under such circumstances, it is critical to capture the nonlinearities associated with its deformation during its operation, thus enabling its successful application.

In terms of modelling the behaviour of CNT, several approaches are adopted in the literature ranging from atomistic simulations to conventional continuum models [3, 4]. Though some of the features of CNT (and its composite) behaviour cannot be addressed by continuum modelling approaches, it is generally observed that such continuum approaches are very useful in understanding their structural behaviour and further can be utilised for rapid structural design purposes involving CNT reinforced composite materials [5–12]. Several researchers have observed that continuum

modeling predicts the mechanics of CNT as observed in experiments [6, 13]. In this context, continuum beam and shell models [5–9, 14] have been applied to model the bending and buckling behaviour of CNT with a good success, while non-local beam and shell models [10, 11] were developed to incorporate size effect in CNT mechanical behaviour. A detailed review of investigations of buckling behaviour of CNT using atomistic and continuum approaches has been documented by Wang et al. [15]. Despite the fact that understanding the mechanics of CNTs require lower-scale modeling techniques, continuum approaches have been extensively applied as such an approach can be utilized as a computationally efficient tool as compared to intensive atomistic simulations. It is from this perspective, a continuum approach is utilized in this work based on VAM to model their nonlinear bending and buckling behavior. The objective of the research is to develop an asymptotically-correct geometrically-nonlinear beam model to analyse bending and buckling behavior of CNT, which can be used to understand its mechanical behaviour under various combined loading conditions.

II. Modeling Approach

In this research, following the work of Harursampath[16], the bending behaviour of CNTs are studied in an analytical framework using VAM [17]. VAM has been used in the recent past typically for dimensional reduction problems; for example, to develop beam and plate models and extensively validated for general or thin-walled beams[18]. This work begins with a three-dimensional (3-D) strain energy functional of a CNT. VAM is used to split a general 3-D nonlinear elasticity problem for a beam-like structure into a (2-D) nonlinear cross-sectional analysis and a 1-D nonlinear beam analysis (as shown in Fig. 2) by taking advantage of certain geometric as well as material-based small parameters inherent to the tube-like structure such as that of the CNT, considered in this paper. From the geometry of the CNT, as shown in Fig. 3a, the natural small parameters in this problem are the thickness-to-radius ratio ($\delta_h = h/R$) and the radius-to-length ratio ($\delta_R = R/l$). So, restricting the present analysis to long thin-walled slender beams (tubes), it is assumed that $\delta_h \ll 1$ and $\delta_R \ll 1$, where R is a characteristic cross-sectional dimension i.e. radius, l is the

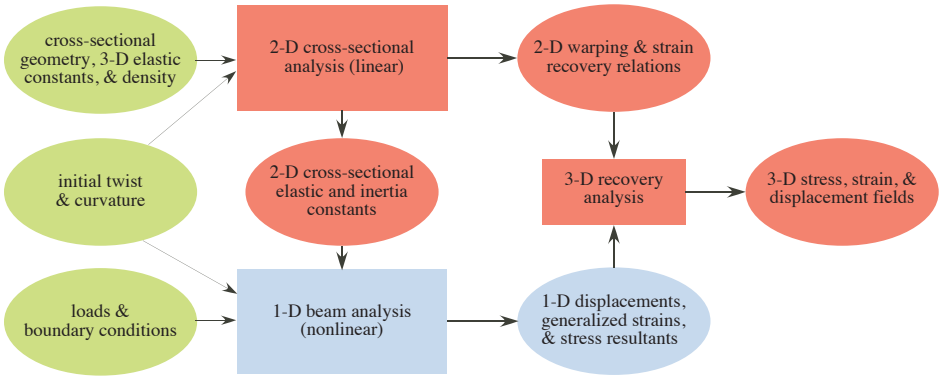

Fig. 2 Summary of beam analysis procedure using VAM

wavelength of deformation and h is the wall thickness, also referred to as t in the existing literature. In this work, the moment-curvature relationship obtained from the cross-sectional analysis (i.e. mean tubular in the beam constitutive law) is nonlinear due to the inherent geometric and structural characteristics. Further, this nonlinearity is analyzed in detail by applying it to a beam-like model of CNT. It is observed that the ovalization of the CNT is captured through the reduction in the bending stiffness, obtained from the 2-D cross-sectional analysis. Local buckling phenomena is also captured through the nonlinear bending response.

A. Cross-sectional modeling of CNT

The present work considers an equivalent tubular structure in lieu of the CNT for the analysis having an outer radius of R_o and inner radius of R_i as shown in Fig. 3.

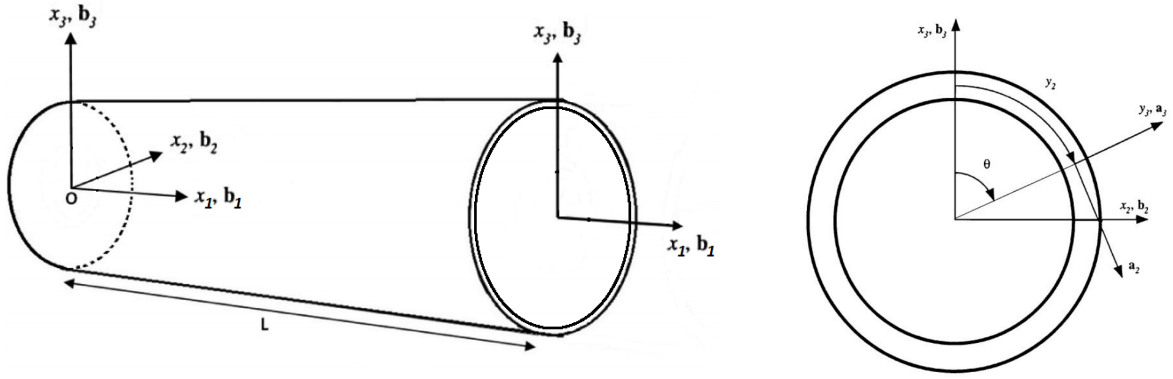

(a) Schematic of the slender prismatic beam model of CNT **(b) Cross section of CNT**

Fig. 3 Beam configuration and coordinate systems

B. Beam Kinematics

The Cartesian coordinate measures x_i and the corresponding unit vectors $\mathbf{b}_i$ are directed as indicated in Fig. 3. For the tubular structure as shown in Fig. 3a, in order to take advantage of the thin nature of the wall, the best way forward is a transformation with the help of cross-sectional arc length y_2, the thickness coordinate y_3 along with the corresponding unit vectors $\mathbf{a}_2(y_2)$ and $\mathbf{a}_3(y_2)$. Also, the domain of the tubular beam is such that $0 \leq x_1 \leq L$, $-\pi R \leq y_2 \leq \pi R$, and $-\frac{h}{2} \leq y_3 \leq \frac{h}{2}$. Then, the position vector of any point for the undeformed beam in an inertial reference frame, $\hat{\mathbf{r}}$ is given as

$$\hat{\mathbf{r}}(x_1, x_2, x_3) = \mathbf{r}(x_1) + x_2\mathbf{b}_2(x_1) + x_3\mathbf{b}_3(x_1) = y_1\mathbf{a}_1 + (R + y_3)\mathbf{a}_3(y_2) \tag{1}$$

where $\mathbf{r}$ is the position vector of any point along the reference line at $x_1 = y_1$. After deformation, the particle that had position vector $\hat{\mathbf{r}}$ in the undeformed state now has the position vector $\hat{\mathbf{R}}$ in the deformed state. Another Cartesian basis $\mathbf{B}_i$ and a curvilinear basis $\mathbf{A}_i$ are specified for the deformed configuration at each point along $\mathbf{R}$ and are relat ed to $\mathbf{b}_i$ through $\mathbf{B}_i = C_{ij}^{Bb}\mathbf{b}_j$. The position vector of an arbitrary point in the deformed state denoted by $\hat{\mathbf{R}}(x_1, x_2, x_3)$ can

now be expressed as

$$\hat{\mathbf{R}}(x_1, x_2, x_3) = y_1\mathbf{a}_1 + u_i(y_1, y_2, y_3)\mathbf{b}_i + (R + y_3)\mathbf{a}_3 \tag{2}$$

The 3-D Green strain is

$$\Gamma = \frac{1}{2}(A^T A - I_3) \tag{3}$$

where I_3 is the 3×3 identity matrix, and A is the mixed-basis component matrix of the deformation gradient tensor such that

$$A_{ij} = \mathbf{B}_i \cdot \mathbf{G}_k\mathbf{g}^k \cdot \mathbf{b}_j \tag{4}$$

where $\mathbf{G}_k$ are the covariant base vectors of the deformed configuration and $\mathbf{g}^k$ are the contravariant base vectors of the undeformed configuration. A here is derived as:

$$A = \begin{bmatrix} 1 + u_1' & \left(\frac{R}{R+y_3}\right)u_{1,2} & u_{1,3} \\ u_2' & 1 + \left(\frac{R}{R+y_3}\right)(u_{2,2} + \frac{u_3}{R}) & u_{2,3} \\ u_3' & \left(\frac{R}{R+y_3}\right)(u_{3,2} + \frac{u_2}{R}) & 1 + u_{3,3} \end{bmatrix} \tag{5}$$

where $()'$ is used when a quantity is differentiated with respect to x_1 or y_1 and subscripts '2' and '3' refer to partial derivatives with respect to y_2 and y_3, respectively.

C. Zeroth-Order Approximation

Using the 3-D elasticity model, the strain energy per unit volume is obtained as

$$U_{3D} = \frac{1}{2}E_{ijkl}\Gamma_{ij}\Gamma_{kl} \tag{6}$$

which is written assuming that the material is linearly elastic satisfying the generalized Hooke's law, i.e., $\sigma = \mathcal{D}\Gamma$ where Γ is the 3-D strain matrix which obtained from Eq. (3), $\sigma = \begin{bmatrix}\sigma_{11} & \sigma_{12} & \sigma_{13} & \sigma_{22} & \sigma_{23} & \sigma_{33}\end{bmatrix}^T$ and the matrix $\mathcal{D}$ is the symmetric matrix of elastic material stiffness coefficients. The strain energy, which would be subjected to minimization with the help of small parameters, can be written as

$$U = \frac{1}{2}\int_0^L \langle \Gamma^{\mathcal{T}}\mathcal{D}\Gamma\rangle dx_1 \tag{7}$$

where $\langle\cdot\rangle = \oint(\cdot)\, dx_2 dx_3$ It is assumed that maximum strain is $O(\epsilon)$, where $\epsilon << 1$. A preliminary order-of-magnitude analysis is performed, retaining only the leading-order terms in the energy. For the zeroth-order approximation, the

minimization of energy gives rise to the following form of the 3-D displacement field:

$$\begin{aligned} u_1^0(y_1, y_2, y_3) &= \overbrace{q_1(x_1)}^{O\left(\frac{\epsilon R}{\delta_R}\right)} \\ u_2^0(y_1, y_2, y_3) &= \overbrace{q_2(x_1)}^{O\left(\frac{\epsilon R}{\delta_R}\right)} + \overbrace{q_3(x_1)\cos\theta}^{O\left(\frac{\epsilon R}{\delta_R^2}\right)} - \overbrace{q_4(x_1)\sin\theta}^{O\left(\frac{\epsilon R}{\delta_R^2}\right)} \\ u_3^0(y_1, y_2, y_3) &= \overbrace{q_5(x_1)}^{O(\epsilon R)} + \overbrace{q_4(x_1)\cos\theta}^{O\left(\frac{\epsilon R}{\delta_R^2}\right)} + \overbrace{q_3(x_1)\sin\theta}^{O\left(\frac{\epsilon R}{\delta_R^2}\right)} \end{aligned} \tag{8}$$

where $\theta = \frac{y_2}{R}$. The classical 1-D degrees of freedom extracted above are rigid-body-like displacements of the tube cross section due to extension (q_1), torsion (q_2) and bending (q_3 and q_4). In addition, there is a circumferential uniform radial displacement (q_5) which could be excited, for example, by a pressure differential between the inside and the outside of the tubular section.

Due to the circular symmetry of the tube, bending in any one direction is similar to that in any other. As such, one of the two bending degrees of freedom (e.g., q_4) can be dropped, for simplicity, without affecting any desired information. The most direct excitation for q_5 is evidently from a pressure loading. From an asymptotic analysis of the energy functional, it can be shown that the pressure required to excite q_5 of $O(\epsilon R)$ is $O(E\delta_h\epsilon)$, where E is the order of elements of $\mathcal{D}$. However, tubes are rarely subjected to such high pressures in practice. It is observed that in the absence of internal or external pressure, as in the current study, q_5 is of an order higher than indicated above for tubes made of known anisotropic materials under all normal beam loading. Thus, the 1D degrees of freedom which need to be retained are q_i.

D. First-Order Approximation

The variational asymptotic methodology that is being followed in the present work, is derived from Ref. [16]. The 3D displacement field for the first-order approximation is given by

$$u_i = u_i^0 + \overline{w}_i(x_1, y_2, y_3) \tag{9}$$

where, $\overline{w}_i$ is the 3D warping field of the cross section, which includes both out-of-plane warping, $\overline{w}_1$, and the in-plane warping, $\overline{w}_2$ and $\overline{w}_3$. The warping variables are subjected to the constraints

$$\langle \overline{w}_i(x_1, x_2, x_3)\rangle = 0, \qquad \langle \overline{w}_{2,3}(x_1, x_2, x_3) - \overline{w}_{3,2}(x_1, x_2, x_3)\rangle = 0 \tag{10}$$

If $\overline{w}_i(y_1, y_2, y_3)$ are the warping measures along $\mathbf{a}_i$ of an arbitrary material point, t Here, it is important to note that

the representation of the warping field is normal to the local shell surface and consists of the following terms

$$\overline{w}_\alpha(x_1, y_2, y_3) = w_\alpha(x_1, y_2) + y_3\phi_\alpha(x_1, y_2) + \Delta_\alpha(x_1, y_2, y_3) \tag{11a}$$

$$\overline{w}_3(x_1, y_2, y_3) = w_3(x_1, y_2) + \Delta_3(x_1, y_2, y_3) \tag{11b}$$

where $\alpha = 1, 2$. The $\Delta_i, i = 1, 2, 3$ represent the unknown variation and the remaining components in the equations (11a) and (11b) are warping and local rotations "averaged" across the thickness. As the warping field is split, it needs to satisfy additional constraints as mentioned below:

$$\int_{-\frac{h}{2}}^{\frac{h}{2}} \Delta_\alpha(x_1, y_2, y_3)\, dy_3 = 0, \tag{12}$$

$$\int_{-\frac{h}{2}}^{\frac{h}{2}} \Delta_3(x_1, y_2, y_3)\, dy_3 = 0, \tag{13}$$

and

$$\int_{-\frac{h}{2}}^{\frac{h}{2}} \Delta_{\alpha,3}(x_1, y_2, y_3)\, dy_3 = 0 \tag{14}$$

These constraints are required to be satisfied in addition to the constraints provided in Eq. (10) which are enforced due to the extraction of rigid body and uniform radial displacements of the cross section at the zeroth-order approximation. Also, note that w_i are warping measures averaged across the thickness and ϕ_α are the local rotation variables.

The zeroth-order displacement field, Eq. (8), and the warping field, Eqs. (11a) and (11b), are substituted into the displacement field, Eq. (9), which is then substituted into Eq. (3) to obtain the first-order approximation to the 3D strain field. It should be noted that no a priori assumptions were made on the order-of-magnitude of any of the warping variables. However, the material limitation of small stains $\Gamma_{i3} = O(\epsilon)$ requires each of the large terms in the strain is compensated by other such terms in the same strain component. Thus, the following relations are established, from the

large terms in Γ_{13}, Γ_{23}, Γ_{12} and Γ_{22}, respectively:

$$\begin{aligned}
\phi_1 &= \overbrace{-q_3'\sin\theta}^{O\left(\frac{\epsilon}{\delta_R}\right)} \overbrace{-q_3'\phi_2\cos\theta}^{O\left(\frac{\epsilon^2}{\delta_R\delta_h}\right)} + \overbrace{\phi_{1\epsilon}(x_1,y_2)}^{O(\epsilon)} \\
\phi_2 &= \overbrace{\frac{w_2}{R}}^{O\left(\frac{\epsilon}{\delta_h}\right)} + \overbrace{Rw_{2,22}}^{O\left(\frac{\epsilon}{\delta_h}\right)} + \overbrace{\phi_{2\epsilon}(x_1,y_2)}^{O(\epsilon)} \\
w_{1,2} &= \overbrace{q_3'\phi_2\sin\theta}^{O\left(\frac{\epsilon^2}{\delta_R\delta_h}\right)} \overbrace{-q_3'\cos\theta}^{O\left(\frac{\epsilon}{\delta_R}\right)} + \overbrace{w_{1\epsilon,2}}^{O(\epsilon)} \\
w_3 &= \overbrace{-Rw_{2,2}}^{O\left(\frac{\epsilon R}{\delta_h}\right)} + \overbrace{w_{3\epsilon}(x_1,y_2)}^{O(\epsilon R)}
\end{aligned} \tag{15}$$

Subscript ϵ in Eq. (15) denotes thickness-averaged local rotations which are $O(\epsilon)$ and thickness-averaged warping variables which, when non-dimensionalized with respect to R, are $O(\epsilon)$. Note that $w_{1\epsilon}$ and $w_{3\epsilon}$ are both indicated to be $O(\epsilon R)$ at this stage. However, certain other considerations, to be described below, would limit them to be of higher order.

For the thin walls under consideration, a plane stress state has been shown to be asymptotically correct and the 3D strain measures can be represented in the form of 2-D shell strain measures as shown

$$\Gamma_{\alpha\beta} = \epsilon_{\alpha\beta} + y_3\rho_{\alpha\beta} \tag{16}$$

where $\epsilon_{\alpha\beta}$ are the membrane strains and $\rho_{\alpha\beta}$ are the middle surface bending curvatures, where, $\alpha = 1, 2$ and $\beta = 1, 2$. Hence, by inspection of $\Gamma_{\alpha\beta}$, the relation between 2D (shell) measures and the 1D (beam) measures is established. The membrane strains are

$$\begin{aligned}
\epsilon_{11} &= \gamma_{11} + w_1' + O\left(\epsilon^2, \frac{\epsilon^2\delta_R}{\delta_h}, \frac{\epsilon^2\delta^2}{\delta_h^2}\right) \\
\epsilon_{22} &= \frac{w_{3\epsilon}}{R} + O(\epsilon\delta_h) \\
2\epsilon_{12} &= w_{1\epsilon,2} - R\kappa_1 + O(\epsilon\delta_h)
\end{aligned} \tag{17}$$

while the changes in curvature are

$$\begin{aligned}
\rho_{11} &= O\left(\frac{\epsilon}{R}\right) \\
\rho_{22} &= \phi_{2,2} + \left(\frac{\epsilon}{R}\right) \\
2\rho_{12} &= O\left(\frac{\epsilon}{R}, \frac{\epsilon\delta_R}{R\delta}\right)
\end{aligned} \tag{18}$$

where

$$\gamma_{11} = \sqrt{[(1 + u_1^{0\prime})^2 + u_2^{0\prime 2} + u_3^{0\prime 2}]} - 1 \tag{19}$$

is the 1D extensional strain and κ_1 is the 1D twist per unit length. The higher-order terms indicated in Eqs. (17) and (18) are all of the same order, as treated here. However, the orders of the omitted higher-order terms are all explicitly indicated so that the reader knows the range of applicability of the theory developed in this paper.

As the 3-D strains are related to the 3-D shell strain measures, the 2-D strain energy density (i.e., energy per unit middle surface area) can be derived and represented as

$$U_{2D} = \int_{-\frac{h}{2}}^{\frac{h}{2}} U_{3D}\, dy_3 = \frac{1}{2} \begin{Bmatrix} \epsilon_{11} \\ \epsilon_{22} \\ 2\epsilon_{12} \\ \rho_{11} \\ \rho_{22} \\ 2\rho_{12} \end{Bmatrix}^T \begin{bmatrix} A & B \\ B^T & D \end{bmatrix} \begin{Bmatrix} \epsilon_{11} \\ \epsilon_{22} \\ 2\epsilon_{12} \\ \rho_{11} \\ \rho_{22} \\ 2\rho_{12} \end{Bmatrix} \tag{20}$$

where A, B and D are the 2-D membrane, bending and coupling stiffness matrices (3×3), respectively. The beam strain energy density is given by $U_{1D} = \int_{-\pi R}^{\pi R} U_{2D}\, dy_2$. From this, the unknown warping field is obtained by minimizing strain energy functional subjected to the global warping constraints mentioned in Eq. (10). Upon substituting the warping solution in U_{2D} and performing the cyclic integration about y_2, U_{1D} is obtained, which is referred to as one dimensional beam strain energy density correct up to the first order. Recall that $w_{1\epsilon}$ and $w_{3\epsilon}$ were both allowed to be as large as $O(\epsilon R)$ because the preliminary estimation indicated that to be their largest possible magnitude. Now, that will be disproved using the method of proof by contradiction. Note that $w_{3\epsilon}$ appears only in ϵ_{22}, while $w_{1\epsilon}$ appears only in $2\epsilon_{12}$. These would imply that the energy could be minimized with respect to ϵ_{22} and $2\epsilon_{12}$. This, in effect, would mean that the stress resultants N_{22} and N_{12} are zero. However, the solution which results for the warping field has a discontinuity along y_2 in $w_{1\epsilon}$ due to the estimation $w_{1\epsilon} = O(\epsilon R)$; and violates the constraint $\langle w_3 \rangle = 0$ due to the estimation $w_{3\epsilon} = O(\epsilon R)$, invalidating both of these preliminary estimations. In physical terms, a discontinuous solution is valid for a tubular beam with a longitudinal slit or an open circular cylindrical shell. A slit also allows for a much larger twist necessitating the consideration of nonlinear extension-twist coupling, known as trapeze effect and Vlasov-like end effects at first order approximation itself. In the present case, the CNT doesn't have any slit, so we can consider $w_{1\epsilon}$ and $w_{3\epsilon}$ are both of an

order higher than ϵ. Therefore, the first-order approximation to the shell strain energy density is

$$U_{2D} = \frac{1}{2} \times \begin{Bmatrix} \gamma_{11} + \psi \\ -R\kappa_1 \\ \phi_{2,2} \end{Bmatrix}^T \begin{bmatrix} A_{11} & A_{16} & B_{12} \\ A_{16} & A_{66} & B_{26} \\ B_{12} & B_{26} & D_{22}(\rho) \end{bmatrix} \begin{Bmatrix} \gamma_{11} + \psi \\ -R\kappa_1 \\ \phi_{2,2} \end{Bmatrix} \tag{21}$$

where $\psi(x_1, y_2) = w_1'$.

The beam strain energy density (energy per unit length of the tube) is given by $U_{1D} = 2\pi R\langle U_{2D}\rangle$. In order to carry out this integration, we need to obtain ψ and ϕ_2 (the unknown functions of y_2 in Eq. (21). From Eqs. (12)-(14), the constraints of further relevance (those can be expressed in terms of ψ and/or ϕ_2 are

$$\begin{aligned} q_3'\phi_2' \sin\theta + \rho\phi_2 \sin\theta - \rho\cos\theta &= \psi_{,2} \\ \langle\psi\rangle &= 0 \\ \langle\phi_2 \cos\theta\rangle &= 0 \\ \langle\phi_2 \sin\theta\rangle &= 0 \end{aligned} \tag{22}$$

where ρ is the bending curvature which can be expressed in terms of the reference line displacements. As we consider slender CNT tube-like structures, we may neglect the term involving ϕ_2 (as a higher-order end effect) in the first of the above equations. In the present formulation, the unknown variables Δ_i do not appear in the energy and hence the constraints associated with those unknown variables are superfluous. They would however, be important in the cases when higher order terms are retained. Further, minimization of the energy leads to the following set of two differential equations, after the elimination of the Lagrange multipliers used to ensure the satisfaction of the four constraints recently defined in Eq. (22):

$$\begin{aligned} R^3\rho\sin^2\theta A_{11}\psi - R\cos\theta B_{12}\psi_{,\theta} + R^2\rho\sin^2\theta B_{12}\phi_{2,\theta} + R\sin\theta B_{12}\psi_{,\theta\theta}\cos\theta D_{22}\phi_{2,\theta\theta} + \sin\theta D_{22}\phi_{2,\theta\theta\theta} &= 0 \\ -R\rho\cos\theta + R\rho\sin\theta\phi_2 - \psi_{,\theta} &= 0 \end{aligned} \tag{23}$$

Note that the 1D extensional and torsional strains do not enter the above equations. Hence, the warping variables ϕ_2 and ψ are independent of the 1D extensional and torsional strains. Periodic coefficients render the above equations difficult to solve in closed form. These differential equations are solved numerically using shooting method for comparison with a Fourier series approximation, to be obtained below.

A one-term Fourier series solution is first attempted. The simplest admissible function for ϕ_2 resulting in non-zero

solution is $\phi_{s2} \sin 2\theta$. This is substituted into the constraint Eq. (22) to obtain

$$\psi = \psi_0 + R\rho[(\phi_{s2}/6)(3\sin\theta - \sin 3\theta) - \sin\theta] \tag{24}$$

The integration constant $\psi_0 = 0$ on imposing the constraint $\langle\psi\rangle = 0$. Minimizing the energy with respect to ϕ_{s2} and defining

$$\mu = D_{22}/R^2 A_{11} \tag{25}$$

results in the following solution:

$$\phi_{s2} = \frac{9(R\rho)^2}{5(R\rho)^2 + 72\mu} \tag{26}$$

Closed-form solutions thus obtained for the perturbations, $\overline{w}_i$, to the zeroth-order displacements, u_i^0, and it is verified that their order-of-magnitude are not lower than that of the preliminary estimations. The first-order approximation to the displacement field (including all terms up to $O(\epsilon R)$) is

$$\begin{aligned}
u_1^I &= q_1 - q_3'\{(R+y_3)\sin\theta - \frac{3(R\rho)^2}{10(R\rho)^2 + 144\mu} \times [3(R - y_3)\sin\theta - (R + 3y_3)\sin 3\theta]\} \\
u_2^I &= q_2 + q_3\cos\theta - \frac{3(R\rho)^2}{5(R\rho)^2 + 72\mu}(R - 3y_3)\sin 2\theta \\
u_3^I &= q_3\sin\theta + \frac{6(R\rho)^2}{5(R\rho)^2 + 72\mu} R\cos 2\theta
\end{aligned} \tag{27}$$

Results for two- and four-term solutions to ϕ_2 are similarly obtained but not explicitly listed here, both because they are negligible in influence on the results in this paper and the complexity of the equations involved.

III. Results and Discussion: Cross-Sectional Analysis

All results presented in this section correspond to the one-term solution obtained for ϕ_2 in Eq. (26), unless otherwise specified.

A. Beam Stiffness

After obtaining the beam strain energy correct up to the first order, the 1-D beam constitutive law is summarized here, which is expressed in terms of the beam strains, namely the extension γ_{11}, twist κ_1 and bending curvature ρ. It is important to note that due to the axisymmetry present in the structure, bending stiffness in both the cross-sectional Cartesian coordinate directions would be the same and hence only one of them is chosen for representation of the

constitutive law in Eq. (28). Coefficients A_{11}, A_{16} and A_{66} are functions of material parameters and cross-sectional geometric parameters defined by Harursampath [16].

$$\mathcal{U}_{1D} = \frac{1}{2}\begin{Bmatrix} \gamma_{11} \\ \kappa_1 \\ \rho \end{Bmatrix}^T \begin{bmatrix} 2\pi R A_{11} & -2\pi R^2 A_{16} & 0 \\ -2\pi R^2 A_{16} & 2\pi R^3 A_{66} & 0 \\ 0 & 0 & S_{33}(\rho) \end{bmatrix} \begin{Bmatrix} \gamma_{11} \\ \kappa_1 \\ \rho \end{Bmatrix} \tag{28}$$

where, the nonlinear bending stiffness, S_{33}, is given as follows:

$$S_{33}(\rho) = \pi R^3 A_{11}\left[1 - \frac{9(R\rho)^2}{144\mu + 10(R\rho)^2}\right] \tag{29}$$

It is important to note that the second term in the expression above, for S_{33}, reduces the bending stiffness with increasing bending curvature and is the source for the well-known nonlinearity. The only factor influencing this nonlinearity is the ratio of the square of the non-dimensional bending curvature, R_ρ, to μ. The definition of μ in Eq. (25) shows that it is a non-dimensional measure of the resistance of the cross section to flatten/deform in its own plane. A small μ results in a cross section which is very easily deformed causing highly nonlinear behavior. The limiting cases are

- $\mu = 0$ which results in a semi-membranous (infinitesimally thin) tube with 90% reduction from the linear value of S_{33}, independent of the bending curvature; and
- $\mu \to \infty$ which results in a rigid cross section tube with no nonlinearity.

In general, μ is inversely proportional to δ_h^2 making thinner tubes more non-linear than the thicker-ones, thus, depicting the need for accommodating this nonlinearity in the analysis of CNT which are thin-walled tubular structures. The smallest value of μ is independent of the material used and is only a function of the geometry.

There is another stiffness parameter, β, defined as

$$\beta = \frac{B_{12}}{\sqrt{D_{22}A_{11}}} \tag{30}$$

and it is a non-dimensional measure of the material coupling between the axial strain and change in shell in-plane curvature which contributes to the energy through S_{33}. However, it shows up only in the two-or-more-term Fourier series solutions and is seen to be a higher-order effect. Further, β is zero for isotropic materials and for the present work involving CNTs. Nonetheless, this coupling factor would be important if one considers a coated CNT beam, for example when modelling a CNT reinforced in a epoxy matrix [19].

B. Bending Moment

From the beam strain energy density, the expression for the bending moment can be obtained through partial differentiation of the energy density, $\mathcal{U}_{1D}$, with respect to the bending curvature ρ.

$$M = \frac{\partial \mathcal{U}_{1D}}{\partial \rho} = \pi R^3 A_{11} \rho \left\{ 1 - \frac{9(R\rho)^2 \left[144\mu + 5(R\rho)^2 \right]}{2\left[72\mu + 5(R\rho)^2 \right]^2} \right\} \tag{31}$$

C. Limit-Moment Instability

The limit moment, M_{l}, defined by the point at which the bending curvature increases with decrease in bending moment can be obtained by maximizing the moment with respect to the elastic curvature. Further, following the work of Harursampath [16], the critical moment, M_{l}, corresponding to the limit-load type instability

$$M_{\text{l}} = 4.223 R^2 A_{11} \sqrt{\mu} \tag{32}$$

In this approach, there are no *ad hoc* assumptions which at times lead to conservative results where limit moment is predicted to be lower than the value obtained from an asymptotically-correct approach.

D. Local Buckling

It has been observed that there is a mode of local failure initiation which precedes the theoretical limit moment in many practical designs. This is caused by localized buckling of the circular shell in the region of maximum compression. The stability analysis is focused on this zone of initial buckling. The maximum compressive stress resultant occurs at $\theta = 90^\circ$ and is given by

$$(-N_{11})_{\max} = -A_{11} \times \left[\gamma_{11} - R\rho + \frac{6(R\rho)^3 - 18\beta\sqrt{\mu}(R\rho)^2}{72\mu + 5(R\rho)^2} \right] + R A_{16} \kappa_1. \tag{33}$$

This gives us the local buckling stress resultant to perform the stability analysis based on the non-linear results presented in this paper. Following the work of Harursampath [16], the critical stress at the center of any initial buckles is nearly equal to that of uniform axial compression. Further, accounting for the change in shell curvature due to nonlinear bending and using the current notation, we obtain

$$\begin{aligned} N_{\text{buckling}} &= 2(1 + R\rho_{22}|_{\theta=90^\circ})(\beta + \chi)\sqrt{\mu} A_{11} \\ &= 2\left[\frac{72\mu - 13(R\rho)^2}{72\mu + 5(R\rho)^2} \right](\beta + \chi)\sqrt{\mu} A_{11} \end{aligned} \tag{34}$$

where

$$\chi = \sqrt{\frac{D_{11}\overline{A}_{22}}{D_{22}A_{11}}} \tag{35}$$

and

$$\overline{A}_{22} = A_{22} - \frac{A_{12}^2}{A_{11}}. \tag{36}$$

The critical bending curvature at which the local bucking initiates, is then derived by equating the right-hand sides of the Eqs. (33) and (34), setting $\gamma_{11} = 0$ and $\kappa_1 = 0$ for pure bending. The smallest possible real solution for the cubic equation in ρ is sought and a closed-form expression is obtained. The moment at which the local bucking initiates is then calculated as

$$M_b = \pi R^2 A_{11}\overline{\rho}_{lb}\left[1 - \frac{9\overline{\rho}_{lb}^2\left(144\mu + 5\overline{\rho}_{lb}^2\right)}{2\left(72\mu + 5\overline{\rho}_{lb}^2\right)^2}\right] \tag{37}$$

where

$$\overline{\rho}_{lb} = \frac{2}{3}\sqrt{\mu}\left[22\beta + 13\chi - \mathcal{R}(C_2) + \sqrt{3}\mathcal{I}(C_2)\right] \tag{38a}$$

$$C_2 = \sqrt[3]{C_1 + \sqrt{C_1^2 - \left[54 + (22\beta + 13\chi)^2\right]^3}} \tag{38b}$$

$$C_1 = 81(22\beta + 13\chi) + (22\beta + 13\chi)^3 - 243(\beta + \chi) \tag{38c}$$

$$\tag{38d}$$

In the above equations, the principal value of $exp(\log x/n)$ is to be attributed to $\sqrt[n]{x}$. It should be noted that this estimate of the local buckling load needs to be checked with the results from a fully nonlinear stability analysis.

E. Cross-Sectional Deformation: Ovalization

The flattening of the cross section, $\Delta = -w_3|_{\theta=90^\circ} - w_3|_{\theta=-90^\circ}$, is given by

$$\Delta = \frac{6R^3\rho^2}{5(R\rho)^2 + 72\mu}. \tag{39}$$

Parametric equations for the cross section change from $x_2 = R\sin\theta$ and $x_3 = R\cos\theta$ to

$$X_2 = R\left(1 - \frac{\phi_{s2}}{2}\right)\sin\theta + R\frac{\phi_{s2}}{6}\sin 3\theta \tag{40a}$$

$$X_3 = R\left(1 + \frac{\phi_{s2}}{2}\right)\cos\theta + R\frac{\phi_{s2}}{6}\cos 3\theta. \tag{40b}$$

In this case, we do not making any assumption restricting the deformation of the circle to an ellipse, as done in some classical literature, such as Ades [20]. Fig. 4b shows the difference at the limit-moment instability, assuming other modes of failure have not already occured at a smaller moment. The shape of the deformed cross-section at the limit moment is independent of the material properties and geometry of the CNT. A closer observation reveals that the limit moment instability occurs almost immediately after there is a change in the sign of shell curvature at the points of maximum compression and tension ($\theta = \pm 90°$).

F. Results for a Stand-Alone CNT under Bending

A hollow CNT beam of wall thickness, $h = 0.066$ nm and radius $R = 1.5$ nm is considered for the analysis. The geometry and material data used for the study are taken from the reference [21]. The CNT is assumed to be isotropic and linearly elastic with material properties given by its Young's modulus $E_{\text{CNT}} = 5.5$ TPa and Poisson's ratio, $\nu_{\text{CNT}} = 0.19$. Using the expression in Eq. (31), the moment-curvature relation is plotted in Fig. 4a along with the version obtained using linear analysis. The cross-section of the undeformed and deformed CNT subjected to a bending moment is also shown in Fig. 4b.

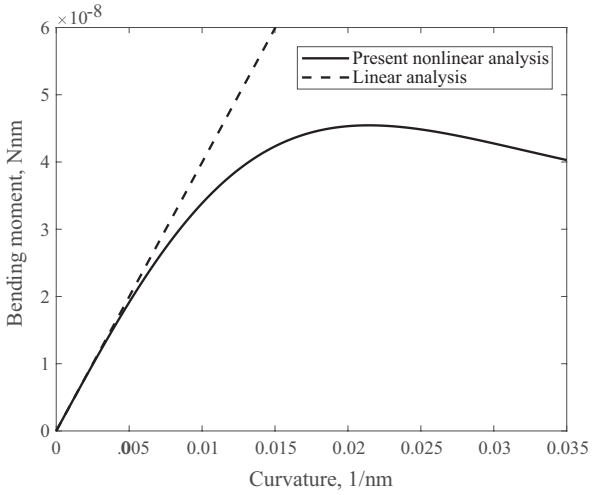

(a) Plot of the nonlinear bending moment-curvature relation of a CNT

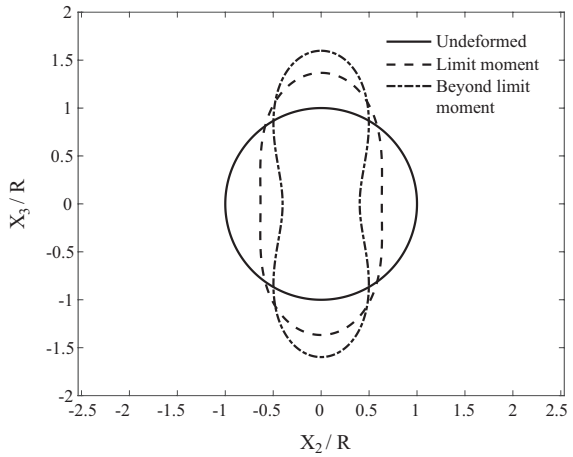

(b) Cross-sectional deformation of the CNT showing the ovalization phenomenon which leads to nonlinearity in the moment-curvature relation

Fig. 4 Nonlinear bending analysis of a CNT

From the results reported in Fig. 4a, it can be clearly observed that the variation of the bending moment with respect to the curvature is nonlinear due to the inherent hollow thin-walled geometrical characteristics of the CNT. After the initial linear regime, a gradual nonlinearity is observed, which is attributed to the gradual ovalization of the cross-section, i.e., reduction in the beam height in the direction of the bending results in reduced bending stiffness of the beam. A limit moment, M_{l}, is observed beyond which the bending stiffness of the CNT starts decreasing. In other words, the beam softens when it undergoes further bending after the limit bending moment.

G. Comparison with Results in the Literature

In this section, the present results are compared against the results reported in various studies in the literature. Several articles addressed the nonlinear bending and buckling behaviour of CNTs using continuum elasticity approach, Molecular Dynamics MD simulations and Finite Element Method FEM. A detailed review of different modelling techniques adopted for analyzing the mechanical behaviour of CNTs can be found here [3].

The results obtained using the present asymptotic approach are compared with the results obtained using MD simulation, FEM and continuum shell modelling [13, 15, 21]. In particular, the variation of critical curvature corresponding to local buckling with respect to the CNT diameter is compared. The following geometric properties of the CNT are utilized [21]: wall thickness, $h = 0.066$ nm; diameter of the CNT is varied from $d = 0.5$ nm to 3 nm. The results obtained are plotted against the literature results in Fig. 5. The result of critical curvature by Yakobson et al. [13] is given by $2.352 \times t/d^2$, while the results obtained by Cao et al. [21] are described as follows: From MD simulations, they obtained the following expression for critical curvature by curve fitting, $\kappa = 0.0738/d^2$ and from FEM analysis using shell elements, they obtained a curve-fitted expression given by $\kappa = 0.1076/d^2$.

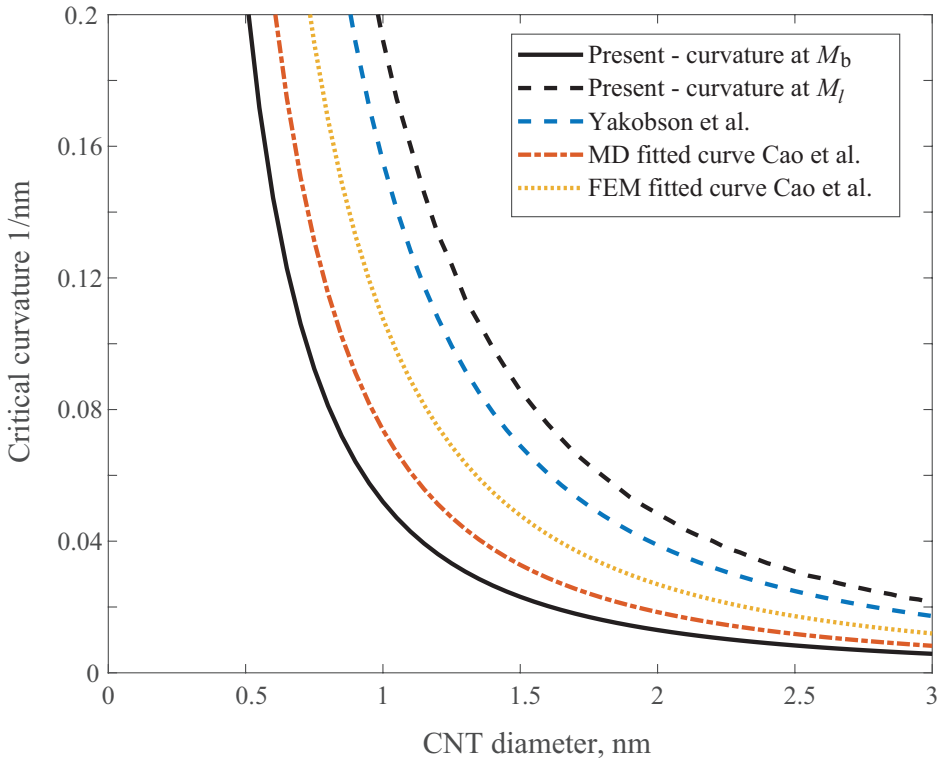

Fig. 5 Comparison of results obtained using present formulation to those obtained from MD, FEM, and other results present in the literature

Figure 5 plots the curvature corresponding to the limit moment, M_l as a function of the CNT diameter. From the comparison, it can be observed that the present results on the buckling curvature are in close agreement with the literature results obtained from MD simulations. It can also be seen that the FEM and continuum shell models

overestimate the curvature at buckling and that is because of the *ad hoc* assumptions involved in the analysis, thus, supporting the argument made in Sec. III.C. It is also interesting to note that the buckling curvature and the curvature corresponding to the limit moment obtained from the present study forms the upper and lower bounds on the variation plots. Thus, it can be concluded that the present continuum modelling approach using VAM provides a good prediction for the nonlinear bending and buckling behaviour of CNTs.

H. Effect of wall thickness of CNT

In the literature, effective wall thickness of CNT is still an issue to be resolved, as several works report varying effective wall thicknesses of the CNT. Hence, to explore the effect of CNT wall thickness, the present CNT beam model is used for a parametric study where the thickness is assigned values ranging from $h = 0.02$ nm to $h = 0.16$ nm. The results of the analysis are summarized in Fig. 6.

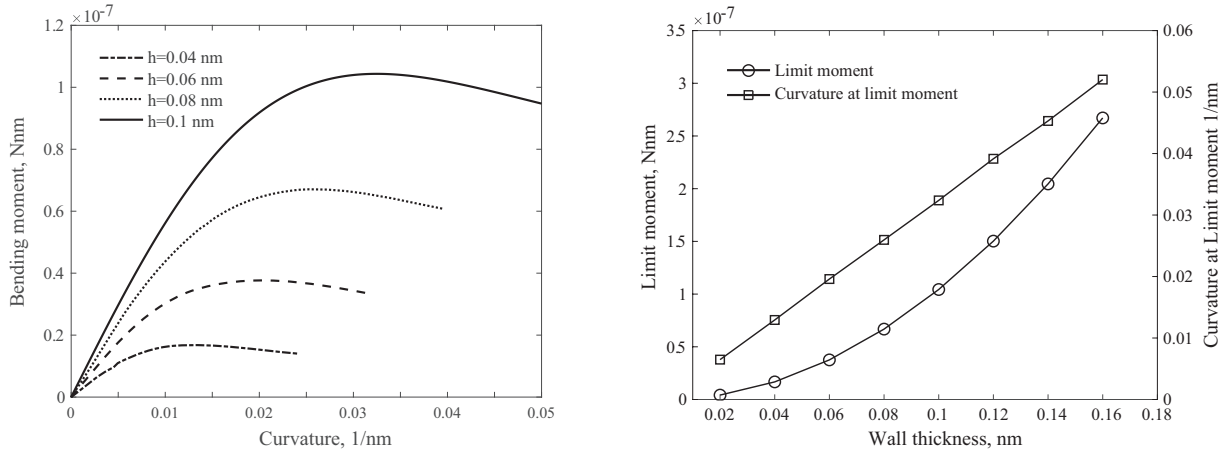

(a) Nonlinear bending moment-curvature relation **(b) Limit moment vs. wall thickness**

Fig. 6 Effect of wall thickness on CNT bending behaviour

Figure 6a represents the nonlinear variation of the bending moment with increase in the curvature.From the Fig. 6b, it is observed that increasing the wall thickness increases the load carrying capability of the CNT beam. The limit moment and the corresponding curvature at the limit moment (M_l) increase monotonically with the thickness of the wall. This is attributed to the fact that, as the thickness increases, the geometric contribution of the beam towards its bending stiffness increases. Nonetheless, it is worth noting that the limit moment has a quadratic dependence on the wall thickness, whereas the curvature at the limit moement varies linearly. More importantly, when the thickness of the wall is increased, the associated nonlinearity (Brazier effect) is less pronounced and becomes negligible if the thickness is increased beyond a limit in comparison with the diameter. It is also worth noting that the solutions provided in this work take advantage of a small parameter, thickness-to-radius ratio. The solutions are sensitive to this parameter and are only valid for small wall-thickness-to-radius ratios. To summarize, it can be concluded that the influence of wall

thickness on the bending behaviour is significant, thus warranting an accurate representation of the equivalent CNT thickness whenever it is modelled in the continuum framework.

IV. Summary and Outlook

A CNT is modelled as a slender beam structure using VAM and its bending and buckling behavior was studied. From the nonlinear moment-curvature relation, the solutions for the limit moment and the moment corresponding to local buckling are reported and compared against literature results. The present results have shown that the model developed using VAM was able to capture the nonlinear bending behaviour reasonably well in terms of critical curvatures, when compared with the MD simulations and other related works in the literature. Effect of varying wall thickness on its bending capability was reported which indicated the crucial influence that the choice of equivalent wall thickness possesses on the bending characteristics of CNTs. Work is in progress to integrate the beam model with a one-dimensional theory[22], which can further be used to study the deformation behaviour and stress state in CNTs (and their composites) under arbitrary loading conditions. Further, atomistic aspects such as van der Waals interactions are being explored for inclusion in the continuum model, which is important especially when ovalisation of the cross-section occurs bringing the walls closer. Researchers in the past have worked to develop continuum models which account for van der Waals interactions such as the work by Liew et al. [23], to understand the buckling behavior of CNTs, but this paper attempts to fill a gap in the literature by using an asymptotically-consistent beam model, considering Brazier effect for CNTs.

References

[1] Feng, E. H., and Jones, R. E., "Carbon nanotube cantilevers for next-generation sensors," *Physical Review B*, Vol. 83, No. 19, 2011, p. 195412.

[2] García, E. J., Hart, A. J., and Wardle, B. L., "Long carbon nanotubes grown on the surface of fibers for hybrid composites," *AIAA journal*, Vol. 46, No. 6, 2008, pp. 1405–1412.

[3] Rafiee, R., and Moghadam, R. M., "On the modeling of carbon nanotubes: a critical review," *Composites Part B: Engineering*, Vol. 56, No. 1, 2014, pp. 435–449.

[4] Pal, G., and Kumar, S., "Modeling of carbon nanotubes and carbon nanotube–polymer composites," *Progress in Aerospace Sciences*, Vol. 80, No. 1, 2016, pp. 33–58.

[5] Pantano, A., Boyce, M. C., and Parks, D. M., "Nonlinear structural mechanics based modeling of carbon nanotube deformation," *Physical review letters*, Vol. 91, No. 14, 2003, p. 145504.

[6] Pantano, A., Parks, D. M., and Boyce, M. C., "Mechanics of deformation of single-and multi-wall carbon nanotubes," *Journal of the Mechanics and Physics of Solids*, Vol. 52, No. 4, 2004, pp. 789–821.

[7] Ru, C., "Column buckling of multiwalled carbon nanotubes with interlayer radial displacements," *Physical Review B*, Vol. 62, No. 24, 2000, p. 16962.

[8] Zhang, Y., Wang, C., and Tan, V., "Buckling of multiwalled carbon nanotubes using Timoshenko beam theory," *Journal of Engineering Mechanics*, Vol. 132, No. 9, 2006, pp. 952–958.

[9] Ru, C., "Effective bending stiffness of carbon nanotubes," *Physical Review B*, Vol. 62, No. 15, 2000, p. 9973.

[10] Sudak, L., "Column buckling of multiwalled carbon nanotubes using nonlocal continuum mechanics," *Journal of Applied Physics*, Vol. 94, No. 11, 2003, pp. 7281–7287.

[11] Zhang, Y., Liu, G., and Wang, J., "Small-scale effects on buckling of multiwalled carbon nanotubes under axial compression," *Physical review B*, Vol. 70, No. 20, 2004, p. 205430.

[12] Yang, J., Ke, L., and Kitipornchai, S., "Nonlinear free vibration of single-walled carbon nanotubes using nonlocal Timoshenko beam theory," *Physica E: Low-dimensional Systems and Nanostructures*, Vol. 42, No. 5, 2010, pp. 1727–1735.

[13] Yakobson, B. I., Brabec, C., and Bernholc, J., "Nanomechanics of carbon tubes: instabilities beyond linear response," *Physical review letters*, Vol. 76, No. 14, 1996, p. 2511.

[14] Vodenitcharova, T., and Zhang, L., "Bending and local buckling of a nanocomposite beam reinforced by a single-walled carbon nanotube," *International journal of solids and structures*, Vol. 43, No. 10, 2006, pp. 3006–3024.

[15] Wang, C. M., Zhang, Y., Xiang, Y., and Reddy, J., "Recent studies on buckling of carbon nanotubes," *Applied Mechanics Reviews*, Vol. 63, No. 3, 2010, p. 030804.

[16] Harursampath, D., and Hodges, D. H., "Asymptotic analysis of the non-linear behavior of long anisotropic tubes," *International journal of non-linear mechanics*, Vol. 34, No. 6, 1999, pp. 1003–1018.

[17] Hodges, D. H., "Nonlinear composite beam theory," *Progress in astronautics and aeronautics*, Vol. 213, 2006, p. 304.

[18] Gupta, M., and Hodges, D. H., "Modeling Thin-Walled Beams using VAM," *58th AIAA/ASCE/AHS/ASC Structures, Structural Dynamics, and Materials Conference*, 2017, p. 1832.

[19] Hadjiev, V., Lagoudas, D., Oh, E., Thakre, P., Davis, D., Files, B., Yowell, L., Arepalli, S., Bahr, J., and Tour, J., "Buckling instabilities of octadecylamine functionalized carbon nanotubes embedded in epoxy," *Composites Science and Technology*, Vol. 66, No. 1, 2006, pp. 128–136.

[20] Ades, C. S., "Bending strength of tubing in the plastic range," *Journal of Aeronautical Sciences*, Vol. 24, No. 2, 1957, p. 605.

[21] Cao, G., and Chen, X., "Buckling of single-walled carbon nanotubes upon bending: Molecular dynamics simulations and finite element method," *Physical Review B*, Vol. 73, No. 15, 2006, p. 155435.

[22] Ponnusami, S. A., Harursampath, D., and Uthandi, A., "Nonlinear modeling of piezocomposite actuators with application to self-actuating flapping wing micro aerial vehicles," *53rd AIAA/ASME/ASCE/AHS/ASC Structures, Structural Dynamics and Materials Conference 20th AIAA/ASME/AHS Adaptive Structures Conference 14th AIAA*, 2012, p. 1966.

[23] He, X., Kitipornchai, S., and Liew, K., "Buckling analysis of multi-walled carbon nanotubes: a continuum model accounting for van der Waals interaction," *Journal of the Mechanics and Physics of Solids*, Vol. 53, No. 2, 2005, pp. 303–326.